*J. Fluid Mech.* (2014), *vol.* 739, *pp.* 465–478.  
doi:10.1017/jfm.2013.633

# Effects of roughness on particle dynamics in turbulent channel flows: a DNS analysis

**Barbara Milici[1], Mauro De Marchis[1],†, Gaetano Sardina[1] and Enrico Napoli[2]**

[1]Facoltà di Ingegneria, Architettura e delle Scienze Motorie, Università degli studi di Enna 'Kore', 94100 Enna, Italy

[2]Dipartimento di Ingegneria Civile, Ambientale, Aerospaziale e dei Materiali, Università degli Studi di Palermo, 90133 Palermo, Italy

(Received 17 June 2013; revised 22 November 2013; accepted 27 November 2013; first published online 2 January 2014)

Deposition and resuspension mechanisms in particle-laden turbulent flows are dominated by the coherent structures arising in the wall region. These turbulent structures, which control the turbulent regeneration cycles, are affected by the roughness of the wall. The particle-laden turbulent flow in a channel bounded by irregular two-dimensional rough surfaces is analysed. The behaviour of dilute dispersions of heavy particles is analysed using direct numerical simulations (DNS) to calculate the three-dimensional turbulent flow and Lagrangian tracking to describe the turbophoretic effect associated with two-phase turbulent flows in a complex wall-bounded domain. Turbophoresis is investigated in a quantitative way as a function of the particle inertia. The analysis of the particle statistics, in term of mean particle concentration and probability density function (p.d.f.) of wall-normal particle velocity, shows that the wall roughness produces a completely different scenario compared to the classical smooth wall. The effect of the wall roughness on the particle mass flux is shown for six particle populations having different inertia.

**Key words:** multiphase and particle-laden flows, particle/fluid flows, turbulent flows

## 1. Introduction

Two-phase flows involving mixtures of gas or vapour or solid particles and liquids are very common in industrial, environmental and scientific applications (steam turbines, plume formation in the atmosphere, pollutant dispersion, etc.) and there are many theoretical, experimental and numerical studies on turbulent flows transporting a dispersed phase (see among others Mohanarangam, Tian & Tu 2008; Balachandar & Eaton 2010; Sardina *et al.* 2012*a*, and references therein).

Important transport processes, including mixing and dispersion of contaminants, in the form of particles, droplets or bubbles, are controlled by the advective action of the fluctuating, turbulent velocity field and by the interaction between the carrier flow and the dispersed phase, even in dilute cases.

Particle dispersion and modulation in turbulent flows are characterized by several phenomena, such as preferential particle concentration, appearing in the form of small-scale clustering and turbophoresis (see among others Narayanan *et al.* 2003;

† Email address for correspondence: mauro.demarchis@unikore.it

Picano, Sardina & Casciola 2009; Toschi & Bodenschatz 2009; Balachandar & Eaton 2010; Sardina *et al.* 2012*a*). Small-scale clustering consists of loss of spatial homogeneity of particle distribution due to the combination of particle inertia and fine-scale turbulent fluctuations, occurring in both homogeneous and inhomogeneous flows. Turbophoresis occurs in all kinds of flows characterized by gradients of turbulence intensity (Caporaloni *et al.* 1975): it is a distinctive feature of wall-bounded flows where particle transfer induced by turbulence generates strong macroscopic particle accumulation at the walls; exhaustive reviews can be found in Marchioli & Soldati (2002), Picano *et al.* (2009), Soldati & Marchioli (2009) and Sardina *et al.* (2012*a*).

Small-scale clustering and turbophoresis are attributed to particles' finite inertia (different from that of the carrier fluid) which prevents them from following fluid trajectories and selectively filters turbulent structures, leading to preferential concentration outside the vortical regions. In wall-bounded turbulent flows these processes are associated with a characteristic particle flux towards the wall: under appropriate conditions, particles may achieve large concentrations at the wall, up to several thousand times the mean value.

Owing to the practical relevance of particle deposition mechanisms in turbulent wall-bounded flows, in the last few decades a lot of works have focused on understanding of the mechanisms involving the coupled interactions between the dispersed phase and the turbulent wall structures. These coherent regions bring particles towards and away from the wall and favour particle segregation in the viscous region (see Marchioli & Soldati 2002; Picano *et al.* 2009; Sardina *et al.* 2012*a*, for a complete review). Previous results (Cerbelli, Giusti & Soldati 2001; Rouson & Eaton 2001; Marchioli & Soldati 2002; Soldati & Marchioli 2009) show that particle deposition is controlled by coherent flow motions (sweep/ejection cycles), linked to the instantaneous realizations of the Reynolds stresses. Owing to inertia, particles are not able to follow the long turbulent quasi-streamwise vortices typical of wall turbulence. Specifically, the inertial particles cross the vortical structures in the proximity of the wall and, driven to the wall by sweeps, accumulate in specific flow regions close to the wall where they tend to stay for long residence times (Reeks 1983; Narayanan *et al.* 2003; Soldati & Marchioli 2009), unable to re-entrain into the outer flow by ejections.

Although small-scale clustering and turbophoresis are commonly separately addressed, they occur simultaneously in wall-bounded flows, representing different aspects of the same preferential accumulation process due to inertial effects, as outlined by Sardina *et al.* (2012*a*). Inertial effects, responsible for filtering out wall turbulent structures, largely depend on the characteristic time scales between the two phases. The relative importance of these time scales is usually expressed by a dimensionless parameter which quantifies the response of the dispersed phase to the perturbations produced by the underlying turbulence, the so-called Stokes number $St$ (Maxey & Riley 1983). It is defined as the ratio between a characteristic relaxation time, which describes the time that a particle needs to adjust to a change in the flow velocity, and a characteristic time scale of the turbulent flow (Balachandar & Eaton 2010).

Turbulent particle-laden flows of engineering and environmental interest are frequently bounded by solid irregular rough walls whose asperities strongly modify the turbulent structures (ejections and sweeps) responsible for wall particle dispersion (Hong, Katz & Schultz 2011; Volino, Schultz & Flack 2011). The spatial inhomogeneity of the height of wall peaks and cavity regions locally destroys the coherent patterns of the flow (see DeMarchis, Napoli & Armenio 2010, and references therein). Besides the change of the turbulent carrier flow field, wall roughness strongly

modifies the dispersed-phase properties. The wall asperities considerably alter not only wall collision processes but also wall collision frequency, as demonstrated previously (Tsuji *et al.* 1987; Sommerfeld & Huber 1999; Sommerfeld & Kussin 2004; Konan, Kannengieiser & Simonin 2009; Konan, Simonin & Squires 2011). Kussin & Sommerfeld (2002) showed that wall roughness enhances the transverse dispersion of the particles and their fluctuating velocities throughout the channel. For such particles, the understanding of these rebound processes seems to be of fundamental importance, in order to compute realistic trajectories and describe particle distribution phenomena.

The foregoing processes are conditioned by the ratio between the particle diameters and the sizes of wall asperities and have different relevance depending on the distribution of the height and position of roughness peaks, effects that have been treated in numerical simulations using a variety of approaches (Konan *et al.* 2011).

Most previous works have adopted a stochastic modelling of particle–rough wall interactions aimed at analysing the effect of the roughness on a colliding particle without describing the deterministic shape of the irregular wall structure: whenever the particle reaches the rough wall, the rebound process is modelled by introducing a smooth virtual inclined wall with a characteristic chosen angle, in order to reproduce the real rebound effects. This virtual wall modelling implicitly assumes that the roughness height is negligible (Sommerfeld & Huber 1999; Squires & Simonin 2006; Konan *et al.* 2009) rather than attempting to model the actual geometrical profile of the rough surface, as done by the authors in this work.

This paper is mainly focused on the investigation of the effects of irregular wall roughness on the dispersed-phase dynamics in particle-laden turbulent channel flows, especially in terms of preferential particle wall accumulation. The statistical properties of particles much heavier than the carrier fluid are analysed by means of direct numerical simulations (DNS) and particle preferential concentration is addressed as a function of the Stokes number.

## 2. The problem formulation and numerical methodology

Two DNS have been performed at relatively low friction Reynolds number $Re_\tau = u_\tau \delta/\nu = 180$, where $u_\tau$ is the friction velocity, $\delta$ the half channel height and $\nu$ the kinematic viscosity. To focus on applications, simulations have been carried out considering air with density $\rho = 1.3$ kg m$^{-3}$ and $\nu = 15.7 \times 10^{-6}$ m$^2$ s$^{-1}$. One simulation involves flow over classical flat wall whereas in the other two-dimensional irregular roughness is set. The roughness shape is obtained through the superimposition of sinusoidal functions with random amplitudes:

$$r(x_1) = \sum_{i=1}^{n} A_i \sin\left(\frac{2i\pi x_1}{L/2}\right) \tag{2.1}$$

where $r(x_1)$ is the wall boundary distance from a horizontal reference surface, $L$ is the channel length, $n$ is the number of sinusoidal functions, $A_i$ and $L/2i$ are the amplitude and the wavelength of the $i$th function, respectively (see Napoli, Armenio & DeMarchis 2008). In the considered case the number $n$ of sinusoidal functions is set to four (see figure 1*a*). The amplitude $A_1$ of the first function is set to 1 and those of the higher-frequency functions are randomly generated in the range [0–1]. The randomly obtained individual sinusoidal functions are shown in figure 1(*b*). Their sum is then successively scaled in order to obtain a value of the averaged absolute deviation $\bar{r}$

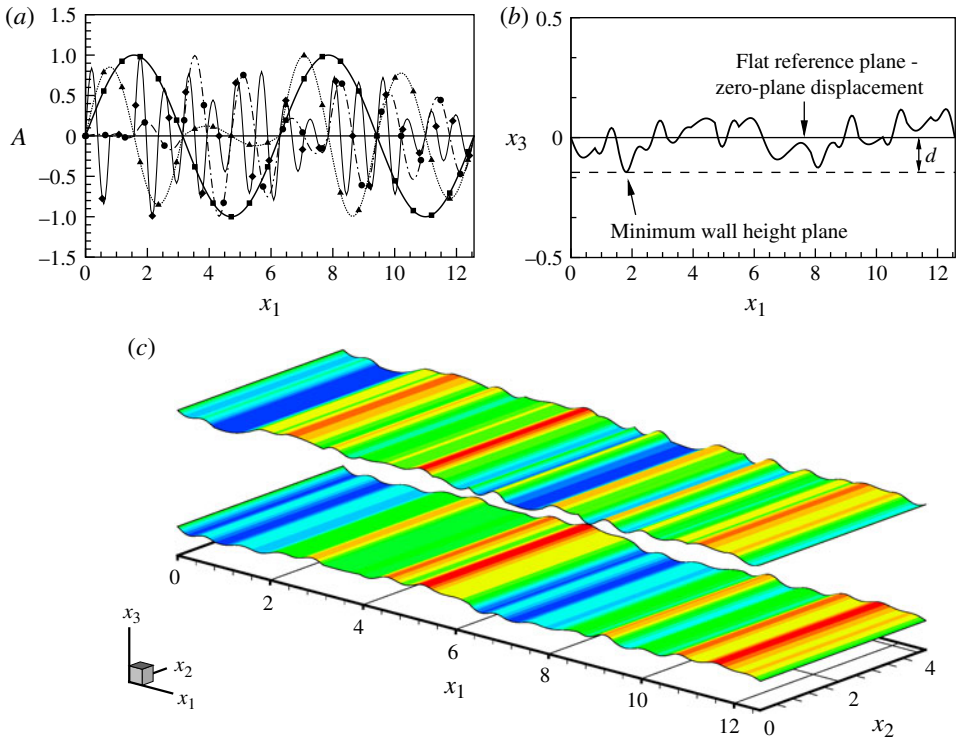


FIGURE 1. (Colour online) (*a*) Plot of the randomly obtained sinusoidal functions (wave periods: -■-, $L/2$; -▲-, $L/4$; -●-, $L/8$; -♦-, $L/16$). (*b*) Sketch of the bottom irregular rough wall, with indication of the reference plane and the displacement height $d$. (*c*) Three-dimensional plot of the rough channel domain (two-dimensional irregular roughness).

equal to $0.05\delta$. The averaged absolute deviation is calculated as:

$$\overline{r} = \frac{1}{\delta}\frac{1}{L}\int_L |r(x_1)|\,\mathrm{d}x_1. \tag{2.2}$$

Both the upper and lower walls are roughened using the procedure described above but, owing to the random generation of the surfaces, the two walls are not symmetric. In order to reproduce a two-dimensional roughness the upper and lower wall geometries are homogeneously applied along the spanwise direction.

The origin of the coordinate system is located at the bottom of the smooth flat channel, which also matches the mean value of the boundary oscillations in the rough channel; the $x_1$, $x_2$ and $x_3$ axes point in the streamwise, spanwise and wall-normal directions, respectively. All results shown below compute the wall-normal distances taking into account the displacement height $d$, due to the roughness (see figure 1*b*). A three-dimensional representation of the rough wall is plotted in figure 1(*c*).

For both the flat and the rough channels the domain length is set to $4\pi\delta$, $(4/3)\pi\delta$ and $2\delta$ in the streamwise, spanwise and wall-normal directions respectively. Periodic boundary conditions are imposed in the streamwise and spanwise directions, while the no-slip condition is enforced at the walls. Due to these boundary conditions, grid points are uniformly distributed in both the $x_1$ and $x_2$ directions, with grid cell dimension set to $\Delta x_1^+ \approx 8$ and $\Delta x_2^+ \approx 5$ (hereafter the superscript $^+$ indicates

distances normalized in wall units $\nu/u_\tau$). A non-uniform mesh spacing is used in the $x_3$ direction, in order to ensure that the distance of the first grid point from the solid walls is less than one wall unit, with a maximum grid spacing of $\sim$6 wall units at the channel centreline. The resulting number of grid points is 256, 128 and 128 in the streamwise, spanwise and wall-normal directions, respectively.

A coupled Eulerian–Lagrangian numerical method is used to perform numerical simulations of the particle-laden turbulent channel flow. Under the basic assumption of negligible back-reaction of the transported phase on the carrier fluid, the standard wall-bounded flow DNS approach is used for the analysis of the fluid-phase motion, based on the Navier–Stokes and continuity equations. In the conventional summation approach the governing equations read:

$$\frac{\partial u_i}{\partial t} + \frac{\partial u_i u_j}{\partial x_j} - \frac{1}{Re_\tau}\frac{\partial^2 u_i}{\partial x_j \partial x_j} + \frac{\partial p}{\partial x_i} + \Pi\delta_{i1} = 0; \quad \frac{\partial u_i}{\partial x_i} = 0, \quad i = 1, \ldots, 3, \tag{2.3}$$

where the variables are made non–dimensional with the friction velocity $u_\tau$ and the channel half-width $\delta$. In (2.3) $x_i$ is the $i$th non-dimensional coordinate, $u_i$ is the $i$th dimensionless velocity component, $t$ is time and $p$ is the kinematic pressure field (pressure divided by density and $u_\tau^2$). The last term is the imposed mean non-dimensional pressure gradient that drives the flow and $\delta_{ij}$ is the Kronecker function ($\delta_{ij} = 1$ for $i = j$, $\delta_{ij} = 0$ for $i \neq j$). In statistically steady-state conditions, the equilibrium between the imposed pressure gradient and the sum of the streamwise components of the lower and upper wall stresses holds, therefore $\Pi = 1$ always (DeMarchis & Napoli 2012).

The momentum and continuity equations (2.3) are resolved using the finite-volume numerical code PANORMUS (www.panormus3d.org), which allows numerical simulations using structured boundary-fitted (curvilinear) grids. The numerical model, which is second-order accurate both in time and space, uses an explicit Adams–Bashforth method for the time advancement of the solution, while a fractional-step technique is used to overcome the pressure–velocity decoupling typical of incompressible flows. The PANORMUS code has been successfully validated for single-phase turbulent channel flows at Reynolds numbers up to $Re_\tau = 395$ (see DeMarchis & Napoli 2012) as well as in environmental fluid mechanics applications (DeMarchis *et al.* 2012; DeMarchis, Freni & Napoli 2013).

In order to address particle dynamics a Lagrangian approach, tracking the dispersed phase, is coupled to the Eulerian DNS solver for the fluid phase. We assume the simplifying hypothesis that every particle is a rigid sphere with diameter much smaller than any active scale of the turbulent flow. Furthermore, a dilute suspension is considered, in order to neglect feedback of particles on the carrier fluid, particle–particle collisions and mutual hydrodynamic interactions (Maxey & Riley 1983). The ratio between the particle and the fluid density is order 1000. These hypotheses lead us to describe the fluid flow surrounding the particles as a Stokes flow. With the previous assumptions, the only significant force acting on the particles, in the absence of gravity, is the viscous Stokes drag (Maxey & Riley 1983). The equations for the Lagrangian evolution of particle positions and velocities thus read:

$$\frac{\mathrm{d}\boldsymbol{v}^p}{\mathrm{d}t} = \frac{3}{4}\frac{\rho}{\rho_p}\frac{C_D}{d_p}(\boldsymbol{u}(\boldsymbol{x}^p(t), t) - \boldsymbol{v}^p) \cdot |\boldsymbol{u}(\boldsymbol{x}^p(t), t) - \boldsymbol{v}^p|, \tag{2.4}$$

$$\frac{\mathrm{d}\boldsymbol{x}^p}{\mathrm{d}t} = \boldsymbol{v}^p \tag{2.5}$$

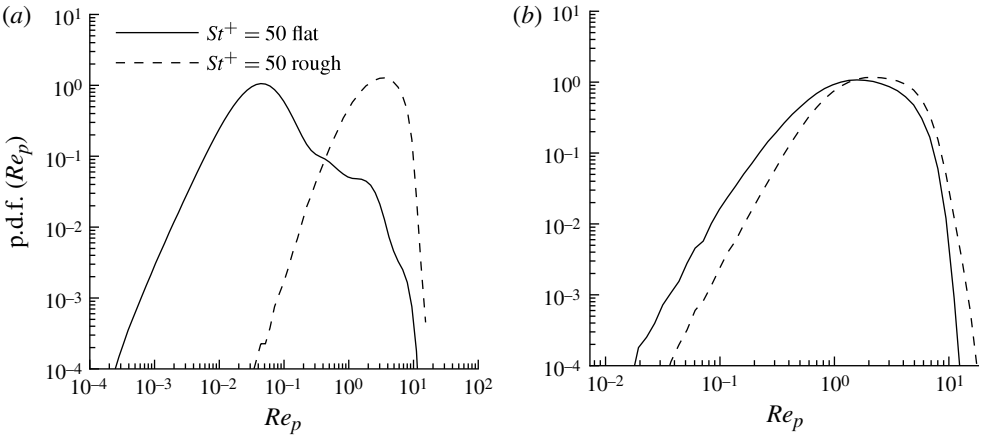


FIGURE 2. p.d.f. of particle Reynolds number in the viscous layer ($0 \leqslant x_3^+ \leqslant 5$) (*a*) and in the buffer layer ($5 \leqslant x_3^+ \leqslant 30$) (*b*), for particles characterized by a viscous Stokes number $St^+ = 50$ for both the smooth flat and the rough simulations.

where $\boldsymbol{u}(\boldsymbol{x}^p(t), t)$ is the fluid velocity at the particle position, $\boldsymbol{v}^p$ and $\boldsymbol{x}^p$ are the non-dimensional velocity and position of the $p$th particle, respectively, $d_p$ and $\rho_p$ the particle diameter and density, $\rho$ the fluid density. $C_D$ is the local drag coefficient that, accounting for the Schiller–Naumann nonlinear correction (Schiller & Naumann 1935), reads:

$$C_D = \frac{24}{Re_p}(1 + 0.15 Re_p^{0.687}) \tag{2.6}$$

where $Re_p = |\boldsymbol{u} - \boldsymbol{v}^p| d_p/\nu$ is the particle Reynolds number. Introducing (2.6) into (2.4) and defining the Stokes number $St$ as the particle response time (or Stokes time) $\tau_p = \rho_p d_p^2/(18\rho\nu)$ divided by a characteristic time scale of the flow, the non-dimensional equations for the Lagrangian evolution of particle positions and velocities read:

$$\frac{\mathrm{d}\boldsymbol{v}^p}{\mathrm{d}t} = \frac{\boldsymbol{u}(\boldsymbol{x}^p(t), t) - \boldsymbol{v}^p}{St}(1 + 0.15 Re_p^{0.687}); \quad \frac{\mathrm{d}\boldsymbol{x}^p}{\mathrm{d}t} = \boldsymbol{v}^p. \tag{2.7}$$

The fluid velocity $\boldsymbol{u}(\boldsymbol{x}^p(t), t)$ is obtained by making use of Taylor expansion of the function $\boldsymbol{u}$ around the fluid node closest to the particle position $\boldsymbol{x}^p$, up to the second-order of accuracy (consistently with the accuracy of the DNS solver). In general cases (Maxey & Riley 1983) the equation for the particle acceleration also includes well-known forces such as buoyancy, added-mass and Basset forces but with the above simplifications and considering particles in the Stokes regime the Lagrangian equations for particle velocity are (2.4) and (2.5) (Narayanan *et al.* 2003). This implies that the Stokes number $St$ is the only parameter defining particle dynamics for a given flow field. In wall-bounded turbulent flows the natural choice for the characteristic time scale is the viscous time scale $\nu/u_\tau^2$; accordingly, the viscous Stokes number is defined as $St^+ = \tau_p u_\tau^2/\nu$. A total of six populations is considered, differing only in the Stokes number ($St^+ = 0.1, 0.5, 5, 10, 25, 50$). The two simulations evolve 100 000 particles per population, in order to keep the same average number concentration.

The Schiller–Naumann nonlinear correction (2.6) starts to be important for $Re_p >$ 0.2, as is well-known. Figure 2 shows the probability density function (p.d.f.) of

| $St^+$ | $\tau_p$ (ms) | $d_p$ (μm) | $Fr_p$ (flat) | $Fr_p$ (rough) |
|---|---|---|---|---|
| 0.1 | 0.08 | 4.71 | 2677.96 | 1599.34 |
| 0.5 | 0.41 | 10.5 | 535.59 | 319.87 |
| 5 | 4.11 | 33.3 | 53.56 | 31.98 |
| 10 | 8.23 | 47.1 | 26.78 | 15.99 |
| 25 | 20.6 | 74.5 | 10.71 | 6.39 |
| 50 | 41 | 105 | 5.35 | 3.19 |

TABLE 1. Inertial particle properties used for the flat and rough simulations.

particle Reynolds number calculated for both the smooth flat and the rough channel simulations in the viscous layer ($0 \leqslant x_3^+ \leqslant 5$) (figure 2*a*) and in the buffer layer ($5 \leqslant x_3^+ \leqslant 30$) (figure 2*b*) relating to the $St^+ = 50$ particles set. Visual inspection of the figures reveals that our simulations have to be carried out using the nonlinear correction.

Regarding boundary conditions of the dispersed phase, particles moving outside of the computational domain in the streamwise and/or spanwise directions are reintroduced via periodicity (i.e. when a particle reaches the artificial boundary of the computational domain it is reintroduced from the opposite side). No other particle injection is considered until reaching the steady state.

The interactions between the dispersed phase and the solid walls of the channel are modelled as purely elastic rebounds, occurring when the particle surface hits the wall. Once the particle positions are evaluated, through (2.7), if the centre of a particle is located at a distance from the wall less than one particle radius, the computed position is adjusted according to elastic collision law. When looking at the rough-wall case, elastic collision methodology has been extended in order to take into account the local slope of the collision plane. The particle-tracking algorithm is parallelized using MPI as for the carrier phase.

In order to avoid possible effects of gravity, the particle Froude number parameter $Fr_p = U_b/(g\tau_p)$ introduced in Sardina *et al.* (2012*b*) should be larger than 1, where $U_b$ is the channel bulk velocity, g is the gravity acceleration. The previous expression can be rearranged (considering $\tau_p = \nu St^+/u_\tau^2$) as $Fr_p = Re_\tau^2 Re_b \nu^2/(St^+ g\delta^3)$ where $Re_b$ is the bulk Reynolds number. Some typical particle properties and parameters are summarized in table 1. Specifically, table 1 clearly shows that the particle Froude number ranges between ∼2600 and 5 (when looking at the flat case), thus supporting the hypothesis of negligible gravity effect. These values are obtained assuming air as carrier phase, $Re_b = 2880$ for the flat case, $Re_b = 1720$ for the rough simulation and a half channel height $\delta = 2$ cm.

## 3. Results

In this section we will use statistical quantities to understand macroscale particle distribution phenomena in connection with the mean features of the carrier-fluid field. Figure 3(*a*) shows the profile of the mean streamwise velocity $U_{x_1}^+ = \langle u_{x_1} \rangle / u_\tau$ across the wall-normal direction $x_3^+$ (angle brackets $\langle \cdot \rangle$ indicate average in time, in the planes of statistical homogeneity and considering symmetry with respect to the mid-plane), obtained in both the flat and the rough wall cases. The two simulations are characterized by the same pressure gradient, therefore the rough-channel flow shows a lower mass flux than the smooth channel. The reduction of the mass

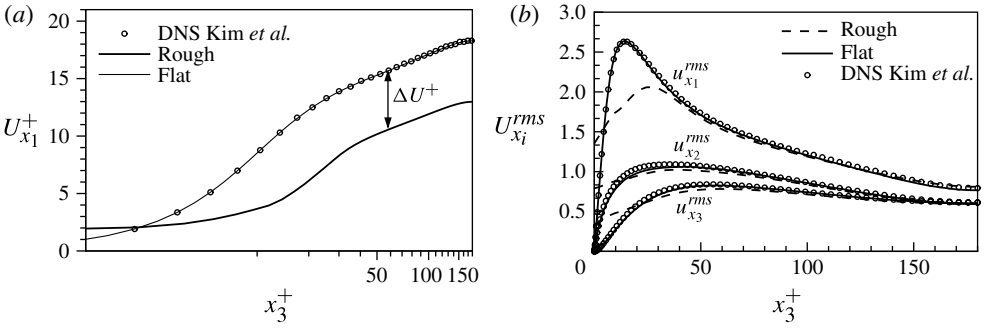


FIGURE 3. (*a*) Mean streamwise velocity $U_{x_1}^+ = \langle u_{x_1} \rangle / u_\tau$ versus the wall-normal direction $x_3^+$ for the flat and rough walls. The symbols are the data extracted from Kim *et al.* (1987) for the flat case. (*b*) Non dimensional r.m.s. of velocity fluctuations: $u_{x_1}^{rms}$ streamwise, $u_{x_2}^{rms}$ spanwise and $u_{x_3}^{rms}$ wall-normal component versus the wall-normal direction $x_3^+$. The symbols correspond to the values of velocity fluctuations in Kim *et al.* (1987) for the flat case.

flux is proportional to the reduction of the streamwise velocity in the bulk region. The difference between logarithmic velocity profiles obtained in flat and rough wall conditions is the so-called *roughness function* $\Delta U^+$, which depends on the geometry and shape of the rough elements, and has been investigated in several works (for a review see Jimenez 2004). Profiles of the fluctuating velocity components are plotted in figure 3(*b*) for both the flat and the rough cases. The plot shows a reduction of root-mean-square (r.m.s.) velocity fluctuations in the wall region, especially for the peak of the streamwise fluctuation. The outer-layer dynamics of the velocity fluctuations is the same in both cases, thus supporting the wall similarity hypothesis (Townsend 1976). In the figures, the symbols represent the data extracted from the DNS database of Kim, Moin & Moser (1987), at the same pressure gradient as for the flat case ($Re_\tau = 180$). As shown in the figure, a very good agreement has been found between our results and the DNS reference data set, so confirming the efficiency of the DNS solver.

In order to analyse the effect of the wall irregularities on particle dispersion, in figure 4 the wall-normal mean number concentration profiles are shown, on a logarithmic scale. We consider the normalized mean particle number concentration $C^* = C/C_0$, defined as the ratio between the number of particles per unit volume and the bulk concentration $C_0$ (i.e. the total number of particles divided by the total volume of the channel). In figure 4(*a*), concerning the flat wall case, particles with finite inertia exhibit maximum number concentration values in the viscous region where the normalized number concentration reaches almost 300 times the value of the pure tracers ($St^+ = 0$) characterized by uniform mean particle number concentration ($C^* = 1$ represented by a dashed line in the figure). This behaviour is a signature of the preferential segregation induced by turbulence (turbophoresis), which generates preferential particle accumulation in the wall region, whose intensity strongly depends on particle inertia. The highest wall concentrations are exhibited by $St^+ = 10, 25, 50$ particles, whose local wall density in the viscous region ($x_3^+ < 5$) reaches values of the order of several thousand times the values in the centre of the channel, where the smallest value of number concentration can be found; the ratio between the wall and the centre concentration is more than $10^4$. Particles with Stokes numbers $St^+ = 10$ and 50 share the same wall and centreline concentrations. These results are in agreement

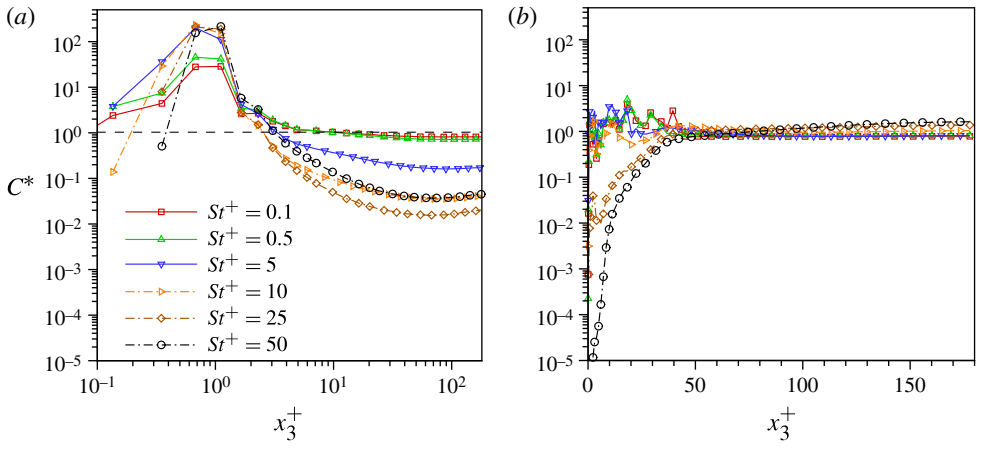


FIGURE 4. (Colour online) Steady-state normalized mean particle number concentration $C^* = C/C_0$ versus wall-normal coordinate $x_3^+$ for the different particle populations. (*a*) Flat case, (*b*) rough case.

with previous DNS findings, obtained at the same friction Reynolds number and similar values of the Stokes number in the flat case (Sardina *et al.* 2012*a*), thus validating the numerical results for the dispersed phase also.

Figure 4(*b*), which displays the particle normalized number concentration profile obtained for the rough channel, suggests that particles tend to avoid the slow flow regions close to the wall for $St^+ = 10, 25, 50$, leading to the total disappearance of the preferential wall accumulation and an increase of the centreline number concentration. Particle depletion in the wall regions increases monotonically with the Stokes number: for the heaviest particles the wall concentration is $\sim 10^5$ times smaller than that for the Lagrangian tracers, while the centreline number concentration has the same order of magnitude as the pure tracers and 200 times the corresponding values obtained for the flat case. A very small amount of turbophoresis is found for the lightest particles. We highlight that number concentration profiles are obtained by averaging over the last 500 $t^+$ of the simulations, thus achieving statistical invariance in time.

Figure 5 gives qualitative evidence of the disappearance of particle preferential concentration close to the wall when the surface roughness is taken into account. The figure shows two instantaneous configurations of the streamwise fluid velocity field together with visualization of particle positions in a wall-normal plane for the flat (figure 5*a*) and rough (figure 5*b*) cases. Contours represent the value of the streamwise velocity field. In order to provide a qualitative representation of the instantaneous particle fluxes towards and away from the wall, we distinguish between particles departing from the wall (particles moving towards the centre of the channel marked with black dots) and particles moving towards the wall (marked with grey dots). In the figure just the particle set characterized by $St^+ = 25$ is shown, which seems to be the most accumulating family, at least for the flat case, as suggested by Soldati & Marchioli (2009). In figure 5(*a*) (flat case), it is clearly shown that relatively few particles tend to populate the centre of the channel, while most of them are localized close to the walls. Conversely, in figure 5(*b*) (rough case), in accordance with the results of Squires & Simonin (2006), a more uniform distribution of particles across the channel is found. Specifically, the particles tend to accumulate in the

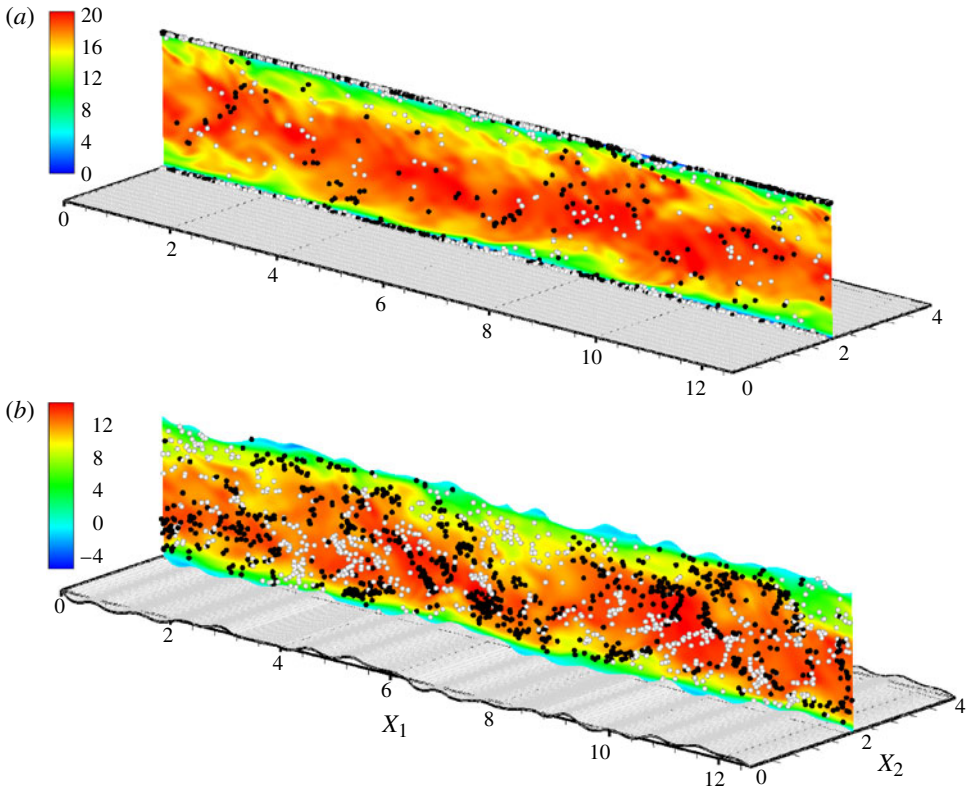


FIGURE 5. (Colour online) Wall-normal slices of an instantaneous configuration of the streamwise velocity field (contours, indicating the non-dimensional instantaneous value) and particles (black particles have positive vertical velocity and move upward, light grey particles have negative vertical velocity and move downward) with $St^+ = 25$ for the flat (*a*) and the rough (*b*) cases.

channel centre, characterized by fast streamwise velocity, and avoid the slow and highly vortical flow regions close to the walls.

The combined effect of the reduction of the particle concentration close to the wall and its augmentation in the channel bulk region deeply affects the total particle mass flux. In order to quantify this flux, we introduce a new physical quantity named *particle bulk Reynolds number* $Re_b^p = V_b^p \delta/\nu$, where $V_b^p$ is the particle bulk velocity, defined as the averaged particle velocity in the streamwise direction ($V_b^p = \sum_{i=1}^{N_p} V_{x_1}^p / N_p$, where $V_{x_1}^p$ is the $p$th particle instantaneous streamwise velocity and $N_p$ is the total number of particles). Figure 6 shows the behaviour of the steady-state particle bulk Reynolds number for the six particle populations, relating to the flat (solid line) and the rough (dashed line) simulations. For $St^+ = 0$, the Lagrangian tracer limit is recovered and the particle bulk Reynolds number is equal to the bulk Reynolds number of the carrier phase ($Re_b^p = 1720$ and $Re_b^p = 2880$ for the rough and the flat case, respectively). Thus, the mass flux for the flat-wall case is larger than that of the rough-wall case, because of the roughness function. In the flat-wall case, the larger the particle inertia (by increasing the Stokes number) the lower the particle mass flux, assuming its minimum value for the most accumulating particles ($St^+ = 25$).

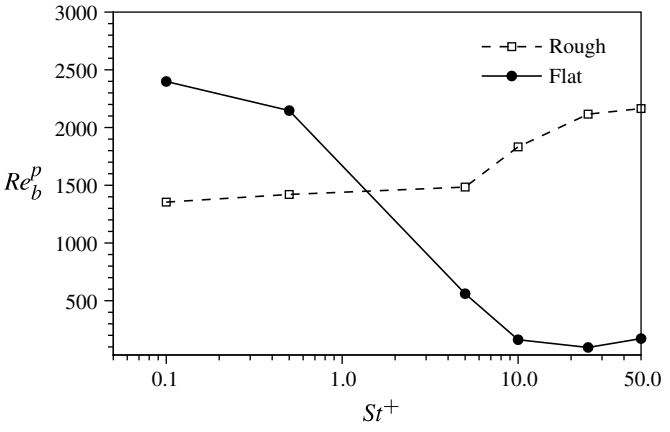


FIGURE 6. Particle bulk Reynolds number $Re_b^p$ as a function of the particle inertia $St^+$ for the flat and rough cases.

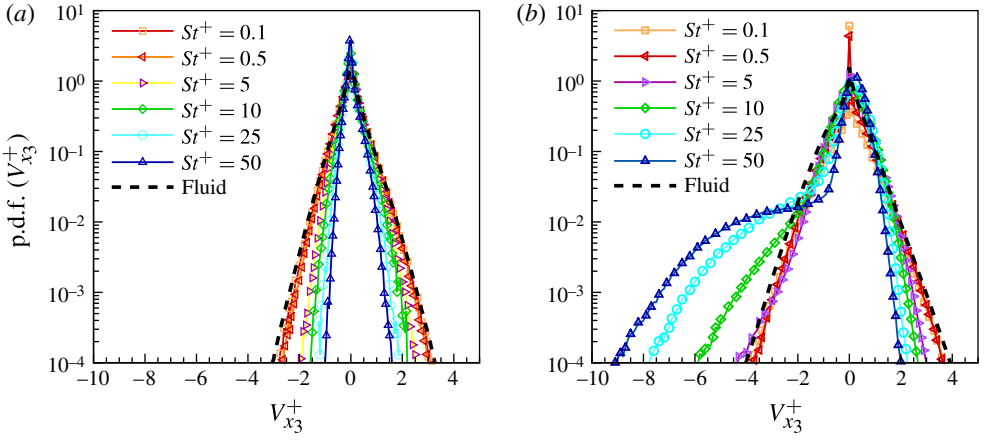


FIGURE 7. (Colour online) p.d.f. of wall-normal particle velocity in the buffer layer ($5 \leqslant x_3^+ \leqslant 30$) at statistically steady state for the flat (*a*) and the rough (*b*) cases.

Conversely, for the rough case the particle mass flux monotonically increases with the Stokes number, an effect which becomes more evident starting from $St^+ = 5$. The maximum ratio between corresponding bulk Reynolds number pairs obtained for the rough and the flat channel is almost 20, which is obtained at $St^+ = 25$. These results clearly imply that transport of sediments or small particulate with non-negligible inertia is more efficient in rough channels than flat ones. The greater efficiency in particle transport for the rough channels is due to the preferential localization of particles in the channel centre, which is characterized by higher streamwise velocities compared to the low-speed wall region.

Figure 7 shows the p.d.f. of the wall-normal particle velocity, $V_{x_3}$, at the steady state in the buffer layer ($5 \leqslant x_3^+ \leqslant 30$) for the flat (figure 7*a*) and the rough cases (figure 7*b*). In the figure $V_{x_3}$ is assumed positive when directed towards the wall and negative in

the opposite case. The thick dashed line is the p.d.f. of the carrier-phase velocity. The other lines in figure 7 indicate the p.d.f.s for the different particle populations. The statistical distribution of figure 7(*a*) shows that intense events departing from the wall (negative particle velocity) are much less frequent for particles than they are for fluid tracers, as shown by the p.d.f. plotted on a semi-logarithmic scale. Particles tend to leave the wall with slow drifting motions rather than fast wall-normal velocities. The larger the inertia the less frequent are the intense particle velocity events, as found by Sardina *et al.* (2012*a*). On the other hand wall-approaching (positive velocity) events are also less frequent than the corresponding velocities of the tracers although their differences are much smaller than the corresponding negative velocity p.d.f. tails. In all cases the mean particle wall-normal velocity vanishes, as it should be at equilibrium.

A completely different scenario appears in the rough channel (figure 7*b*). In this case, the behaviour of the right-hand tails is more or less the same as for the flat-wall case and the particles tend to approach the walls preferentially with slow wall-normal velocities (a behaviour accentuated by increasing the particle inertia). Looking at the left-hand tail it appears that this scenario is qualitatively similar for small and intermediate particles ($St^+ = 0.1, 0.5, 5$), while heavier particles ($St^+ = 10, 25, 50$) are more likely to be entrained by high-velocity departing events. In these cases intense motions directed away from the wall towards the channel centre are much more frequent (up to 100 times) compared to the fluid. This tendency is more evident for the largest particles, in contrast with the flat-wall case where larger inertial particles tend to filter the high-velocity fluctuations.

## 4. Final remarks

DNS of turbulent channel flows at $Re_\tau = 180$ laden with inertial particles are performed over flat and rough walls in order to investigate the effects of the roughness on particle dynamics in turbulent wall-bounded flows. Large particle concentrations are observed near the wall for the classical flat case. The significant finding of our work concerns the effects of wall roughness on inertial particle dynamics. In this case, the opposite situation appears: the inertial particles tend to stay away from the wall region and consequently accumulate at the centre of the channel. The addition of roughness to the wall generates a reduction of the particle accumulation at the wall with respect to the flat turbulent flow driven by the same pressure gradient ($Re_\tau$). This mass flux augmentation is quantified by a new parameter called particle bulk Reynolds number. The reduced wall accumulation can be exploited in applications where an increase of the bulk transport of the particle phase is needed. The present study provides a more general understanding of turbophoresis in cases or geometries more complicated than the simple flat-wall model. The different deposition mechanisms between particles in flat and rough channel flows are driven by the different turbulent structures of the wall turbulence in the two regimes.

## Acknowledgements

The authors acknowledge the support from COST Action MP0806: ‘Particles in turbulence’, COST Action FP1005: ‘Fibre suspension flow modelling’ and SIBSAC PON 01-01844: ‘ An integrated system for sediments remediation and high salinity marine wastewaters treatment’.

## REFERENCES


BALACHANDAR, S. & EATON, J. K. 2010 Turbulent dispersed multiphase flow. *Annu. Rev. Fluid Mech.* **42**, 111–133.

CAPORALONI, M., TAMPIERI, F., TROMBETTI, F. & VITTORI, O. 1975 Transfer of particles in nonisotropic air turbulence. *J. Atmos. Sci.* **32**, 565–568.

CERBELLI, S., GIUSTI, A. & SOLDATI, A. 2001 Ade approach to predicting particle dispersion in wall bounded turbulent flows. *Intl J. Multiphase Flow* **27**, 1861–1879.

DEMARCHIS, M., CIRAOLO, G., NASELLO, C. & NAPOLI, E. 2012 Wind- and tide-induced currents in the stagnone lagoon (Sicily). *Environ. Fluid Mech.* **12** (1), 81–100.

DEMARCHIS, M., FRENI, G. & NAPOLI, E. 2013 Modelling of E. coli distribution in coastal areas subjected to combined sewer overflows. *Water Sci. Tech.* **68** (5), 1123–1136.

DEMARCHIS, M. & NAPOLI, E. 2012 Effects of irregular two-dimensional and three-dimensional surface roughness in turbulent channel flows. *Intl J. Heat Fluid Flow* **36**, 7–17.

DEMARCHIS, M., NAPOLI, E. & ARMENIO, V. 2010 Turbulence structures over irregular rough surfaces. *J. Turbul.* **11** (3), 1–32.

HONG, J., KATZ, J. & SCHULTZ, M. P. 2011 Near-wall turbulence statistics and flow structures over three-dimensional roughness in a turbulent channel flow. *J. Fluid Mech.* **667**, 1–37.

JIMENEZ, J. 2004 Turbulent flows over rough walls. *Annu. Rev. Fluid Mech.* **36**, 173–196.

KIM, J., MOIN, P. & MOSER, R. 1987 Turbulence statistics in fully developed channel flow at low Reynolds number. *J. Fluid Mech.* **177**, 133–166.

KONAN, N. A., KANNENGIEISER, O. & SIMONIN, O. 2009 Stochastic modelling of the multiple rebound effects for particle-rough wall collisions. *Intl J. Multiphase Flow* **35**, 933–945.

KONAN, N. A., SIMONIN, O. & SQUIRES, K. D. 2011 Detached eddy simulations and particle Lagrangian tracking of horizontal rough wall turbulent channel flow. *J. Turbul.* **12** (22), 1–21.

KUSSIN, J. & SOMMERFELD, M. 2002 Experimental studies on particle behaviour and turbulence modification in horizontal channel flow with different wall roughness. *Exp. Fluids* **33**, 143–159.

MARCHIOLI, C. & SOLDATI, A. 2002 Mechanisms for particle transfer and segregation in a turbulent boundary layer. *J. Fluid Mech.* **468**, 283–315.

MAXEY, M. R. & RILEY, J. J. 1983 Equation of motion for a small rigid sphere in a non-uniform flow. *Phys. Fluids* **26**, 883–889.

MOHANARANGAM, K., TIAN, Z. F. & TU, J. Y. 2008 Numerical simulation of turbulent gas-particle flow in a 90 bend: Eulerian–Eulerian approach. *Comput. Chem. Engng* **32**, 561–571.

NAPOLI, E., ARMENIO, V. & DEMARCHIS, M. 2008 The effect of the slope of irregularly distributed roughness elements on turbulent wall-bounded flows. *J. Fluid Mech.* **613**, 385–394.

NARAYANAN, C., LAKEHAL, D., BOTTO, L. & SOLDATI, A. 2003 Mechanisms of particle deposition in a fully-developed turbulent open channel flow. *Phys. Fluids* **15**, 763–775.

PICANO, F., SARDINA, G. & CASCIOLA, C. M. 2009 Spatial development of particle-laden turbulent pipe flow. *Phys. Fluids* **21** (9), 25–39.

REEKS, M. W. 1983 The transport of discrete particles in inhomogeneous turbulence. *J. Aerosol Sci.* **14**, 729–739.

ROUSON, D. W. I. & EATON, J. K. 2001 On the preferential concentration of solid particles in turbulent channel flow. *J. Fluid Mech.* **428**, 149–169.

SARDINA, G., SCHLATTER, P., BRANDT, L., PICANO, F. & CASCIOLA, C. M. 2012*a* Wall accumulation and spatial localization in particle-laden wall flows. *J. Fluid Mech.* **699**, 50–78.

SARDINA, G., SCHLATTER, P., PICANO, F., CASCIOLA, C. M., BRANDT, L. & HENNINGSON, D. S. 2012*b* Self-similar transport of inertial particles in a turbulent boundary layer. *J. Fluid Mech.* **706**, 584–596.

SCHILLER, V. L. & NAUMANN, A. 1935 Uber die Grundlegenden Berechnungen bei der Schwerkraftaufbereitung. *Z. Verein. Deutsch. Ing.* **77**, 318–320.

SOLDATI, A. & MARCHIOLI, C. 2009 Physics and modelling of turbulent particle deposition and entrainment: Review of a systematic study. *Intl J. Multiphase Flow* **35**, 827–839.

SOMMERFELD, M. & HUBER, N. 1999 Experimental analysis and modelling of particle–wall collisions. *Intl J. Multiphase Flow* **25**, 1457–1489.

SOMMERFELD, M. & KUSSIN, J. 2004 Wall roughness effects on pneumatic conveying of spherical particles in a narrow horizontal channel. *Powder Technol.* **142**, 180–192.

SQUIRES, K. & SIMONIN, O. 2006 LES-DPS of the effect of wall roughness on dispersed-phase transport in particle-laden turbulent channel flow. *Intl J. Heat Fluid Flow* **27**, 619–626.

TOSCHI, F. & BODENSCHATZ, E. 2009 Lagrangian properties of particles in turbulence. *Annu. Rev. Fluid Mech.* **41**, 375–404.

TOWNSEND, A. A. 1976 *The Structure of Turbulent Shear Flow*. Cambridge University Press.

TSUJI, Y., MORIKAWA, Y., TANAKAA, T., NAKATSUKASA, N. & NAKATANI, M. 1987 Numerical simulation of gas–solid two-phase flow in a two-dimensional horizontal channel. *Intl J. Multiphase Flow* **13**, 671–684.

VOLINO, R. J., SCHULTZ, M. P. & FLACK, K. A. 2011 Turbulence structure in boundary layers over periodic two- and three-dimensional roughness. *J. Fluid Mech.* **676**, 172–190.